DOI 10.14622/Advances_49_2023_14

Robust method for printed pattern classification and creation of fluid splitting regime maps for gravure printing

Pauline Rothmann-Brumm[1,2] *and Edgar Dörsam*[1,2]

[1] Technical University of Darmstadt, Department of Mechanical Engineering, Institute of Printing Science and Technology, Magdalenenstr. 2, 64289 Darmstadt, Germany

[2] Collaborative Research Center (CRC) 1194 – Interaction between Transport and Wetting Processes, Project C01, Germany

E-mails: rothmann-brumm@idd.tu-darmstadt.de; doersam@idd.tu-darmstadt.de

Short abstract

Hydrodynamic pattern formation in gravure printing is not yet completely understood. Classification of printed patterns serves as a data-driven tool for finding cause-effect-correlations between printing parameters and printed patterns and thus helps to gain a deeper insight into pattern formation phenomena. The focus of this study is hydrodynamic pattern formation that originates from fluid splitting during fluid transfer. We aim to develop a method for pattern classification that is robust against printing defects. Our study is based on a comprehensive image data set created with an industrial web-press. First, a representative data subset is chosen and image preprocessing is performed. Second, classification of printed patterns into three fluid splitting classes, namely point splitting, transition regime and lamella splitting, is conducted by a human observer. The used classification method is optimized compared to previous methods. The main advantage of the new method is that the definition of the transition regime is tunable and thus is more robust against printing defects. Third, the results of the classification are used for the creation of exemplary regime maps which show the regimes of fluid splitting in printing parameter space.

Keywords: rotogravure, pattern formation, fluid splitting, regime maps, robust classification method

1. Introduction and background

Understanding hydrodynamic pattern formation during fluid transfer in printing processes is key for obtaining high-quality printed layers. The quality requirements for the printed layers are usually defined by their application such as graphical printing, printed electronics, functional coatings or bioprinting. An ideal printed layer thus can look very different. Some ideal layers are dominated by dot patterns as in many graphical applications, some ideal layers are smooth and do not have any pattern at all like large-area printed electronics and some ideal layers exhibit a stochastic, biomimetic finger pattern like in printed vascular networks for bioprinting applications. To forecast the printed pattern and to choose the correct printing parameters for each application, a detailed knowledge of cause-effect-correlations between printed patterns and printing parameters is crucial. This knowledge is, e.g., generated by conducting systematic printing experiments and then collect and visualize the results in fluid splitting regime maps. Regime maps in general are a common tool in fluid mechanics for the characterization of fluid flow regimes.

To create fluid splitting regime maps from printing experiments, it is necessary to classify the printed patterns into several types of fluid splitting. From Hübner (1991), we know two types of fluid splitting classes: point splitting and lamella splitting. Brumm, et al. (2021) extended this view to three classes and proved the existence of a transition regime class. In this study, we aim to develop a method for pattern classification that is robust against printing defects. Therefore, we use a large image data set and perform a data-driven analysis on it.

2. Materials and methods

2.1 Image data set

2.1.1 Complete data set

The image data set that serves as a basis for this research was created by Brumm, et al. (2022) on an industrial gravure web-press Bobst Rotomec MW 60-600/250 (Bobst, Mex, Switzerland). The experiments were conducted at printing velocities from 15 to 240 m/min, with water-based and solvent-based gravure inks with four different viscosities on foil and paper substrates, using an electromechanically engraved printing form decorated with full-area patches ("fields") with raster frequencies of 60, 70, 80 and 100 lines/cm and tonal values from 5 % to 100 % in 5 % steps. After high-resolution, color-calibrated scanning at 2 400 dpi and automated digital cutting of the printed samples in the programming language Python, a data set of 48 960 images of size 1 040 px × 1 040 px (11 mm × 11 mm) is obtained. This data set shows a great variety of hydrodynamic pattern formation phenomena from dot raster patterns resulting from "point splitting" to viscous fingering patterns, also called ribbing, resulting from "lamella splitting", see Figure 1. The transition between both types of patterns ("transition regime") is also represented in the data set. The aim of this research is to classify the printed patterns to be able to create fluid splitting regime maps in printing parameter space from the pattern classes and the available metadata in form of printing parameters.

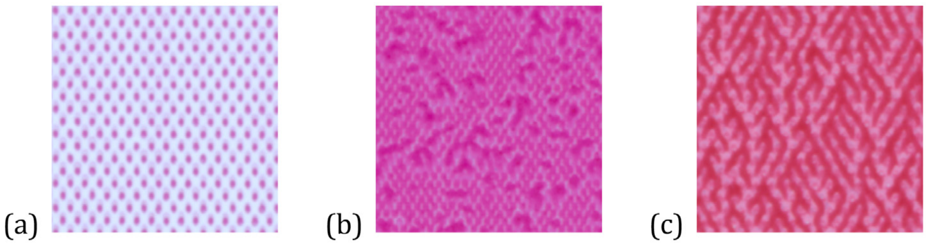

Figure 1: Examples for printed patterns assigned to different fluid splitting classes: point splitting (a), transition regime (b) and lamella splitting (c); each patch has the size 260 px × 260 px (2.75 mm × 2.75 mm)

2.1.2 Data preprocessing

Since in further studies from Brumm, et al. (2021), the manual classification scheme was not very robust against printing defects and thus tended to over exaggerate the amount of samples classified as transition regime, we develop an optimized, robust classification scheme (see section 2.2.). The robust classification scheme requires a simple preprocessing of the data. Each image of size 1 040 px × 1 040 px (11 mm × 11 mm) is divided into 16 equal parts of size 260 px × 260 px (2.75 mm × 2.75 mm). In this way, the data subset is increased from 48 960 images to 783 360 (smaller) images, which are called "subfields" in the following. No other preprocessing steps are performed.

In this study, the fields are divided into 16 subfields, because this results in a good viewing size of each subfield on a 14-inch computer screen such that no zoom-in is needed to observe the printed patterns. This simplifies the manual classification process. A division into 4, 9 or 25 and more subfields would theoretically also be possible. However, a smaller number of subfields per field might need a zoom-in during manual classification to properly see the printed patterns and a larger number of subfields would probably require a higher amount of time for the manual classification, since more subfields would have to be classified.

2.1.3 Selection of a representative data subset

The complete data set is very large so that manual classification of all samples is too time-consuming. Thus, a representative data subset is selected from the complete data set. Only the representative data subset is used for manual classification. The selection is aimed at considering at least samples with extreme values, e.g., with highest, lowest and a medium printing velocity, with the highest and lowest viscosity and with exemplary samples on all substrates and from all printing inks. In total, 26 880 of 783 360 images (3.4 %) were selected for the representative data subset.

2.2 Manual classification

2.2.1 Classification scheme for subfields

Manual classification of the subfields is conducted based on the definition of dot and finger patterns and the manual classification scheme of point splitting, lamella splitting and transition regime as presented in Brumm, et al. (2021). According to their manual classification scheme, a field that only shows “dots”, is classified as point splitting (see Fig. 1a), and a field that only shows “fingers” is classified as lamella splitting (see Figure 1c). Fields that show dots and fingers are classified as transition regime (see Figure 1b). Hereby, one single dot among many fingers or one single finger among many dots is already enough to classify a field as transition regime, making the classification scheme rather harsh. A dot is an “isolated droplet on the printing product on a raster dot position” and a finger is a “liquid ink bridge resulting from viscous fingering on the printed product” and “the smallest finger is as long as the distance between two neighbouring raster dots” (Brumm, et al., 2021).

For this study, we made some changes to the described manual classification procedure to tune its harshness and thus to make it more robust against printing defects. In this work, a printing defect is regarded as a phenomenon that locally changes the pattern within a subfield or a field. This local change of the pattern can lead to a different classification of the subfield or the field, i.e., it corrupts the classification decision. The ideal situation would be to have a data set without any printing defects. In reality, printing defects are common, see Figure 2. Exemplary printing defects include missing dots, “donut” dots, dirt particles, drying patterns, pinholes, inhomogeneous ink distribution, doctor blade stripes etc.

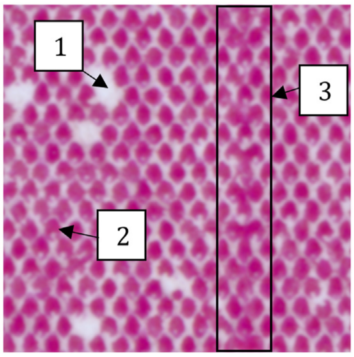

Figure 2: Exemplary printing defects: missing dot (1), “donut” dot (2) and doctor blade stripe (3); the patch has the size 260 px × 260 px (2.75 mm × 2.75 mm)

As an imaginary example, picture a doctor blade stripe that causes an accumulation of printing ink on a printed field. We assume that without the doctor blade stripe, the pattern on the field would be classified as “point splitting”, since the pattern only consists of “dots”. However, in the local region of the doctor blade stripe, the accumulation of ink leads to the formation of “fingers”. This changes the classification decision of the field to “transition regime”, since “dots” as well as “fingers” are present within the field. Consequently, the printing defect corrupted the classification decision of the field.

In Brumm, et al. (2021), classification was performed directly on the fields, whereas in our study, classification is performed on the subfields. The class of the field is then determined from the classification of the subfields using the algorithm from section 2.2.2. Another improvement is the use of an assistance software for the manual classification. This software is an adaption of the Python code "image-sorter2" from Arsenov (2019) and fosters an efficient classification process. Before, a lot of time was lost during organizational tasks during manual classification like opening the correct file and documenting the result in the correct cell in a spreadsheet software. Now, the assistance software automatically shows the next image after an image was classified and it automatically moves the classified image to a folder with the class name. The classification process can be paused and resumed at any time.

2.2.2 Algorithm for classification of fields

The main improvement for increase of robustness against printing defects is the algorithm that determines the class c of a field from the class c_i of its 16 subfields, see Figure 3. Therefore, each c_i is assigned a value a_i according to Equation [1]. All 16 values for a_i are added up for one field and yield a according to Equation [2]. The class c of the field is 1 (point splitting), 2 (transition regime) or 3 (lamella splitting), depending on a and the predefined lower and upper thresholds $a_{\text{tresh},l}$ and $a_{\text{tresh},u}$, see Equation [3].

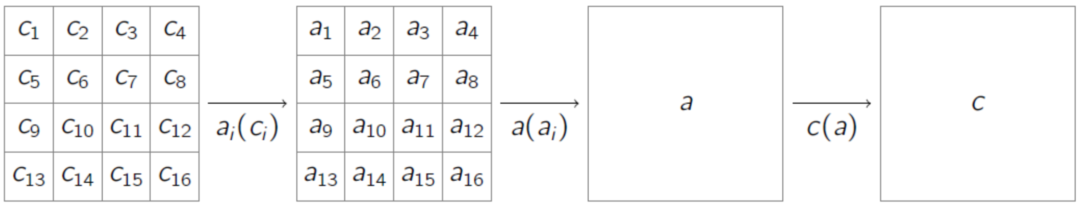

Figure 3: Schematic representation of the algorithm for determining the class c of a field based on the class c_i of its 16 subfields

$$a_i(c_i) = \begin{cases} -1, & c_i = 1 \text{ (point splitting)} \\ 0, & c_i = 2 \text{ (transition regime)} \\ 1, & c_i = 3 \text{ (lamella splitting)} \end{cases} \qquad [1]$$

$$a(a_i) = \sum_{i=1}^{16} a_i \qquad [2]$$

$$c(a) = \begin{cases} 1, & -16 \le a < a_{\text{thresh},l} \\ 2, & a_{\text{thresh},l} \le a \le a_{\text{thresh},u} \\ 3, & a_{\text{thresh},u} < a \le 16 \end{cases} \qquad [3]$$

with $a_{\text{tresh},l} \in \{-15, -14, -13, ..., 0\}$ and $a_{\text{tresh},u} \in \{15, 14, 13, ..., 0\}$

The threshold values $a_{\text{tresh},l}$ and $a_{\text{tresh},u}$ can be used for tuning of the classification decision for the fields. If the thresholds are chosen close to −15 and 15, respectively, the transition regime is very large, whereas the transition regime narrows down for thresholds near zero. With thresholds going towards zero, the majority of subfields must be classified as "transition regime" to make the complete field be classified as "transition regime" as well. This likely eliminates the influence of corrupted classification decisions due to printing defects. However, when choosing a threshold near zero, there might not exist a transition regime any longer, since the criterion is too harsh.

2.3 Creation of exemplary regime maps

From the manual classification of a selected number of subfields from the data subset, we create exemplary fluid splitting regime maps. The regime maps are available in a raw and a processed form. We compare the influence of the upper and lower thresholds on the appearance of the regime maps, especially on the appearance of the transition regime.

3. Results and discussion

3.1 Classification

3.1.1 Distribution of fluid splitting classes within the representative data subset

Within the representative data subset, 9 362 subfields (34.8 %) are classified as point splitting, 3 725 subfields (13.9 %) as transition regime and 13 793 subfields (51.3 %) as lamella splitting.

3.1.2 Distribution of fluid splitting classes within fields

All subfields from the representative data subset were manually classified. When analyzing the class of a subfield over the subfield's position within the field, we observe an inhomogeneity of the distribution of fluid splitting classes within the fields, see Figure 4. It shows how often the subfields of a field were classified as point splitting (Figure 4a), transition regime (Figure 4b) and lamella splitting (Figure 4c). It turns out that the four lower subfields within a field are more often classified as point splitting and transition regime and less often classified as lamella splitting than the rest of the field. Therefore, we assume that the four lower subfields are printed with a lower amount of ink, since a higher ink volume leads towards lamella splitting. We assume that the inhomogeneity originates due to the time dependent excess volume available in the printing nip.

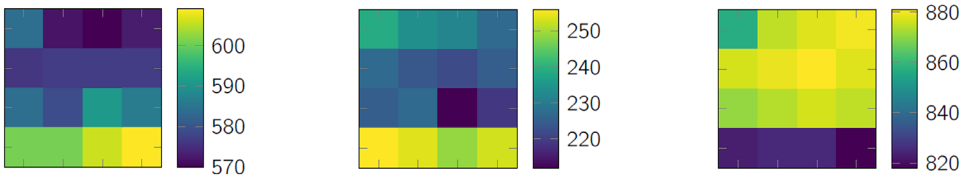

(a) Point splitting (b) Transition regime (c) Lamella splitting

Figure 4: Number of classifications of the 16 subfields into point splitting (a), transition regime (b) and lamella splitting (c) within the fields; the printing direction goes from bottom to top

The printing direction in Figure 4 goes from bottom to top, thus the excess ink volume builds up from bottom to top until it reaches a steady-state. We tried to avoid edge effects and resulting inhomogeneity by discarding the outer 1 mm of each printed field during digital cutting out of the fields, however, 1 mm turns out not to be sufficient.

3.1.3 Tuning the classification of fields

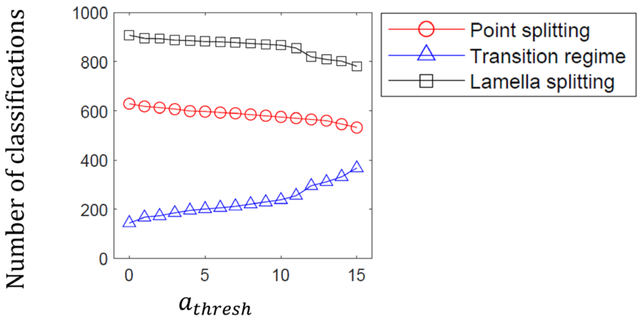

Figure 5: Number of classifications of fields into point splitting, transition regime and lamella splitting over threshold a_{tresh}

As already mentioned, the classification decision of a field based on the classification of its 16 subfields can be tuned via the lower and upper threshold $a_{tresh,l}$ and $a_{tresh,u}$. Figure 5 shows the number of classifications of fields into point splitting, transition regime and lamella splitting over the threshold value $a_{tresh} = |a_{tresh,l}| = a_{tresh,u}$. For simplification reasons, both thresholds are chosen equal in amount. A threshold closer to 15 leads to a higher amount of subfields classified as transition regime.

3.2 Exemplary regime maps

Figure 6 shows exemplary regime maps in raw and processed form for different threshold values. The processing is mainly based on linear interpolation and averaging of regime borders. On the *x*-axis, we see the printing velocity in m/min and on the *y*-axis, we see the tonal value of the printing form in %. The axes span the chosen printing parameter space and the plotted data points show the location of the three fluid splitting regimes: point splitting (red circle), transition regime (blue triangle) and lamella splitting (black square).

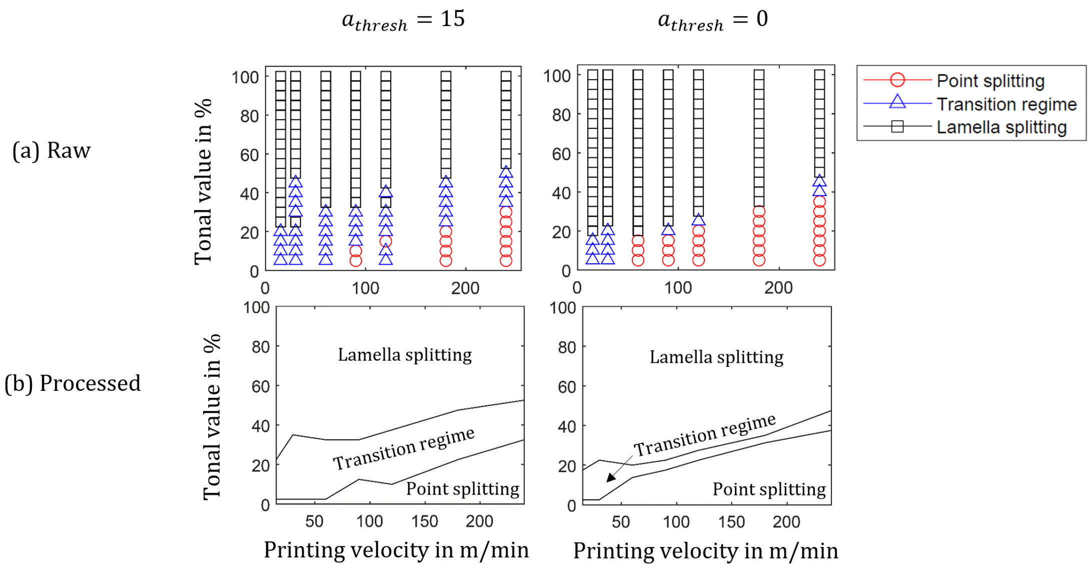

Figure 6: Exemplary regime maps in raw (a) and processed form (b) for two different threshold values

Regime maps with other axes are also possible, e.g., we could use non-dimensional numbers like the capillary number *Ca* on one axis. The regime maps in Figure 6 are based on classified image data from a printing run with id “B3-05” by Brumm, et al. (2022) on coated paper with water-based ink without electrostatic assist. Viscosity of the ink was determined as 17 s with a 4 mm ISO flow cup after DIN EN ISO 2431 (Deutsches Institut für Normung, 2020). Doctor blade angle is 55°. Engraving angle of the electromechanically engraved printing form is HELL engraving angle #2 (59.35°), stylus angle is 120° and raster frequency is 60 lines/cm. A fraction of the data was manually classified by a human observer as explained in section 2.2.1; another fraction was classified using machine learning methods, which is outside the scope of this paper.

From Figure 6 it becomes clear that with a threshold value closer to 15, the transition regime appears much larger than with a threshold value of zero. Thus, the appearance of the regime map can be tuned to the needs of the application. If the printer wants to avoid the transition regime, a threshold value of 15 might be suitable, since the transition regime reaches its biggest extent there. However, if the printer wants to print inside the transition regime, a threshold of zero might be better, since it gives a more precise location of the core of the transition regime.

Apart from tuning the appearance of the transition regime, the threshold leads to a robustness of the transition regime against printing defects when chosen near zero. In case of threshold $a_{tresh} = 0$, a field is only classified as transition regime if all subfields are classified as transition regime ($a_i = 0$) or if all subfields except an even number of subfields are classified as transition regime. The even number of subfields must be half and half point splitting ($a_i = -1$) and lamella splitting ($a_i = 1$) so that their a_i-values add up to zero. As an example, we take a field, of which 14 subfields are classified as lamella splitting and two subfields are classified as transition regime due to a printing defect. This results in $a = 14$. Despite from the printing defects, this field will be classified as lamella splitting, if a_{tresh} is chosen between 0 and 13.

4. Conclusions and outlook

We were able to develop an algorithm for the classification of a field according to the classification of its 16 subfields. We showed that the threshold value a_{tresh} can be used to tune the appearance of the transition regime within fluid splitting regime maps. Besides, threshold values near zero lead to a robustness of the transition regime against printing defects. Exemplary fluid splitting regime maps were created. In future research, the algorithm shall be applied to the complete, available data set and fluid splitting regime maps for a broad variety of printing runs shall be created. The regime maps shall give further insights on the gravure printing process, e.g., on the influence of doctor blade angle, viscosity, substrate, electrostatic assist etc. on hydrodynamic pattern formation and on the resulting fluid splitting class. Moreover, the described methods and algorithms for pattern classification could be transferred to other printing processes.

Acknowledgements

We kindly acknowledge the financial support by the Deutsche Forschungsgemeinschaft (DFG, German Research Foundation) – Project-ID 265191195 – SFB 1194 ‘Interaction between Transport and Wetting Processes’, project C01.

We thank F. Rothmann for fruitful discussion on the developed algorithm.

References

Arsenov, N., 2019. *image-sorter2: one-click image sorting/labeling script*. Github [online] Available at: <https://github.com/Nestak2/image-sorter2> [Accessed 12 April 2023].

Brumm, P., Weber, T.E., Sauer, H.M. and Dörsam, E., 2021. Ink splitting in gravure printing: localization of the transition from dots to fingers. *Journal of Print and Media Technology Research*, 10(2), pp. 81–93. https://doi.org/10.14622/JPMTR-2016.

Brumm, P., Sprinzing, T., Euler, T., Galus, M., Weichmann, A. and Dörsam, E., 2022. Creation of a comprehensive high-resolution image data set on an industrial web press to investigate hydrodynamic pattern formation in gravure printing. In: C. Ridgway, ed. *Advances in Printing and Media Technology: Proceedings of the 48th International Research Conference of iarigai. Greenville, SC, USA, 19–21 September 2022*, pp. 109–115. https://doi.org/10.14622/Advances_48_2022_08.

Deutsches Institut für Normung, 2020. *DIN EN ISO 2431:2020 DE Beschichtungsstoffe – Bestimmung der Auslaufzeit mit Auslaufbechern*. Berlin: DIN.

Hübner, G., 1991. *Ein Beitrag zum Problem der Flüssigkeitsspaltung in der Drucktechnik.* Dissertation. Technische Hochschule Darmstadt. https://doi.org/10.25534/tuprints-00013550.